#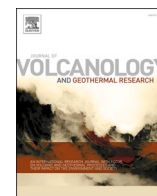 The ghost plume phenomenon and its impact on zenith-facing remote sensing measurements of volcanic SO$_2$ emission rates

N.B. When citing this work, cite the original published paper.

(article starts on next page)

The ghost plume phenomenon and its impact on zenith-facing remote sensing measurements of volcanic SO$_2$ emission rates

D. Skye Kushner [a],[*],[1], Taryn Lopez [a], Christoph Kern [b], Santiago Arellano [c], Nemesio M. Pérez [d], José Barrancos [d]

[a] *Geophysical Institute, Alaska Volcano Observatory, University of Alaska Fairbanks, Fairbanks, AK, United States*
[b] *U.S. Geological Survey, Volcano Science Center, Cascades Volcano Observatory, Vancouver, WA, United States*
[c] *Department of Space, Earth and Environment, Chalmers University of Technology, Gothenburg, Sweden*
[d] *Instituto Volcanológico de Canarias, Tenerife, Canary Islands, Spain*

ARTICLE INFO

ABSTRACT

A large source of error in SO$_2$ emission rates derived from mobile Differential Optical Absorption Spectroscopy (DOAS) of volcanic gas plumes is the uncertainty in atmospheric light paths between the sun and the instrument, particularly under non-ideal atmospheric conditions, such as the presence of low clouds. DOAS instruments measure the SO$_2$ column density along the effective light path, so changes to that pathway directly affect the measured SO$_2$ signal. Due to complex radiative transfer mechanisms when a cloud is between the DOAS viewing position and a volcanic plume, measured plumes can appear spatially offset from their true location, a phenomenon informally referred to as "ghost plumes." In addition to the appearance of ghost plumes, DOAS measurements recorded in non-ideal conditions have poorly characterized errors and are often discarded, limiting the data available to characterize volcanic degassing. In this study we simulate the radiative transfer associated with zenith-facing mobile DOAS traverses using the McArtim radiative transfer model for scenarios when there is a cloud layer between the instrument and the volcanic plume. In total, 217 permutations of atmospheric optical conditions are considered with varying cloud opacities (AOD = 0, 1, 2, 4, 8, 20), plume opacities (AOD = 0, 1, 2, 4, 8), solar zenith angles (SZA = 1°, 30°, 60°), and cloud thicknesses (200, 400, 800 m). We first develop objective criteria for selecting SO$_2$ baseline absorption levels and plume spatial extents. The simulated plume traverses are then integrated to obtain the SO$_2$ cross-sectional burdens which, after multiplication with the wind speed, yield SO$_2$ emission rates. We find large modification in the shape of the modeled cross-sectional burdens even under translucent (low AOD) cloud conditions in our modeled scenarios. Despite modification of the plume shape, the presence of a low cloud layer is typically not a large source of error in the SO$_2$ cross-sectional burden or emission rate obtained from zenith-facing DOAS traverses. We find that all measured cross-sectional burdens simulated using an aerosol-free plume in the above conditions and SZA $\leq$ 30° are within $\pm$25% of the true value.

1. Introduction

Monitoring volcanic sulfur dioxide (SO$_2$) emissions provides insights into subsurface conditions that may precede volcanic eruptions, such as changes in magma supply or conduit permeability (Fischer et al., 2002; Kunrat et al., 2022). After H$_2$O and CO$_2$, SO$_2$ is typically the most abundant volatile species in volcanic plumes and is generally easier to measure than H$_2$O and CO$_2$ due to the negligible SO$_2$ present in the

(unpolluted) background atmosphere (Mather, 2015; Oppenheimer et al., 2014). Differential Optical Absorption Spectroscopy (DOAS), which uses scattered ultraviolet (UV) solar radiation as a light source, is currently the most widely used technique for deriving high-temporal-resolution measurements of volcanic SO$_2$ emission rates (Edmonds et al., 2003; Galle et al., 2003; Galle et al., 2010; Arellano et al., 2021). This method builds upon the Bouguer–Lambert–Beer Law describing the extinction of radiation as it passes through a medium as Eq. (1):

$$I(\lambda) = I_0(\lambda)e^{(-\sigma(\lambda) \times c \times L)}. \tag{1}$$

Here, $I_0(\lambda)$ is the initial light intensity as a function of wavelength λ, $I(\lambda)$ is the light intensity after absorption in the medium, $\sigma(\lambda)$ is the wavelength-dependent absorption cross section of the medium, c is the concentration of the absorbers, and L is the optical path length.

In addition to narrow-band absorption by trace gases (e.g., SO_2), radiation traveling through the atmosphere is subject to scattering on air molecules, in addition to scattering and absorption on aerosols. These scattering and absorption processes are broadband in nature, meaning they affect all wavelengths in a similar way, in this case over a window of several tens of nanometers (nm). The DOAS technique separates the broadband effects from the trace gas absorption by including a low-order polynomial in the spectral analysis, thus effectively high-pass filtering the spectra (Platt and Stutz, 2008). This enables SO_2 to be successfully measured in Earth's atmosphere in the presence of light scattered by gases, aerosol particles, and cloud droplets.

Individual DOAS measurements do not contain information on the spatial distribution of a trace gas in the atmosphere ($c(l)$). The measured absorption is determined by the trace gas slant column density S (SCD), or the concentration integrated along the light path as Eq. (2):

$$S = \int_L^0 c(l) \, dl, \tag{2}$$

Here, dl is a differential element of the optical path. Using this terminology, the Bouguer–Lambert–Beer Law may be formulated for DOAS applications as in Eq. (3):

$$\tau = ln\left(\frac{I_0}{I}\right) = \sum_i \sigma_i \, S_i + P_n. \tag{3}$$

As shown in Eq. (3), the measured optical depth τ is modeled as a linear combination of all trace gases with absorption features in the chosen wavelength region, whereby the absorption cross section σ_i of each species is multiplied by its corresponding column density S_i. Broadband scattering and absorption effects are described by the low-order polynomial P_n. During the DOAS fit procedure, the column densities of the trace gases are varied until a best fit between the measurement of $ln(I_0/I)$ and the model is achieved (Platt and Stutz, 2008). The column density S_i that achieves the best fit to the measurements represents the results of the DOAS measurement.

DOAS-derived SO_2 emission rates are calculated through a multistep process (detailed in Galle et al., 2003) and can be used by volcano observatories to track changes in volcanic emissions over time. A series of individual SO_2 column density measurements are collected while scanning across a plume perpendicular to its propagation direction. Full plume scans can be obtained by moving the DOAS instrument across the plume at a fixed angle (mobile DOAS or zenith-facing mobile DOAS if the telescope is facing directly upward), or the DOAS instrument can scan from horizon to horizon from a fixed position (scanning DOAS). Integration of the SO_2 column densities (in SO_2 molec cm^{-2}) over the plume width (in m) yields the SO_2 cross-sectional burden (in SO_2 molec m^{-1}). Multiplication of this cross-sectional burden by the normal component of plume velocity (equal to wind speed at the plume altitude in m•s^{-1}) yields the emission rate of the desired gas for the volcano (in units of molec s^{-1}, typically converted in terms of masses: t d^{-1} or kg s^{-1}; McGonigle et al., 2005).

When volcanic SO_2 emission rates are retrieved from scanning or mobile DOAS measurements, it is often assumed that the measured light has passed through the volcanic plume to the DOAS telescope along a straight path. However, under real-world conditions photons may travel along complex pathways and may be absorbed or multiply scattered by aerosols or clouds in the atmosphere, complicating the interpretation of retrieved SO_2 column densities and potentially affecting emission rate calculations (Millán, 1980; Williams-Jones et al., 2008). Previous work has highlighted how non-ideal measurement conditions, such as an opaque plume or the presence of clouds between the instrument and

plume, can significantly affect photon paths in and around volcanic plumes and lead to order-of-magnitude errors in derived emission rates (Kern et al., 2010). Recent work by Wagner et al. (2023) has also highlighted that complex radiative transfer pathways can result in pixel saturation, artificially elongated plumes, and other geometric effects for satellite observations of gases that absorb in the UV spectrum. Additionally, scattering of photons that have not passed through a volcanic plume into the instrument field of view may lead to substantial underestimation of SO_2 column densities, an effect commonly referred to as light dilution (Mori et al., 2006; Kern et al., 2010). Because of the potential large and unconstrained errors introduced in DOAS SO_2 measurements collected under non-ideal (e.g., cloudy or foggy) atmospheric conditions, these data are often not collected or used. This can result in limited observations to characterize volcanic degassing — especially for volcanoes often obscured by clouds and fog (e.g., those in the Aleutian Islands [Alaska, USA]).

1.1. Ghost plumes

Further complicating accurate assessments of volcanic SO_2 cross-sectional burdens is the "ghost plume" phenomenon, where a measured plume is geometrically offset from where it is expected or has a modified shape that differs from that of the real plume (Williams-Jones et al., 2008). Ghost plumes occur when a cloud or layer of aerosols is present between the volcanic plume and the DOAS telescope under specific illumination conditions depending on the relative positions of the sun, the plume, scattering cloud, and instrument. During conditions where a cloud layer is beneath a volcanic plume, solar UV radiation that has already passed through the plume can be scattered towards the instrument by the underlying cloud. If the sun is not directly overhead, this can lead to the plume being detected in a position horizontally offset from its expected location, producing a modified cross-sectional burden. Because the ghost plume effect is a result of radiative transfer, this phenomenon is not restricted exclusively to DOAS (either scanning or mobile) measurements and should also occur in other remote spectroscopic techniques used to measure volcanic degassing, including SO_2 cameras and correlation spectrometers (COSPEC; Williams-Jones et al., 2008). Despite the potential ubiquity of this scattering effect, there have not been quantitative studies to assess or identify the impact on field measurements. Hereafter, we concentrate on only zenith-facing mobile DOAS measurements.

The horizontal offset position of a ghost plume relative to the real plume can be resolved through simple trigonometry if several crucial aspects of a traverse are known. Here, we define a "real plume" as the expected vertical projection of a plume when measured with a zenith-facing telescope and assuming ideal radiative transfer, i.e., all photons pass vertically through the overhead plume. The predicted distance between the real volcanic plume and a ghost plume can be calculated by knowing the solar zenith angle φ (SZA), the solar azimuth relative to the plume, and the altitude difference between the plume and a condensed layer (e.g., cloud or fog). Fig. 1 illustrates a case where the path of the zenith-facing mobile DOAS traverse is parallel to the solar azimuth, meaning that the traverse is moving directly toward or away from the sun. In this scenario the ghost plume maximum SO_2 column density would be geometrically expected to occur offset from the plume by distance d in Eq. (4), where h is the difference in altitude between plume and scattering cloud, as shown in in Fig. 1:

$$d = h \times tan(\varphi) \tag{4}$$

2. Methods

To assess the utility of real-world SO_2 emission rate measurements obtained where there is a cloud layer present between the DOAS telescope and the volcanic plume, we simulate zenith-facing DOAS measurements under realistic conditions. We use a radiative transfer model
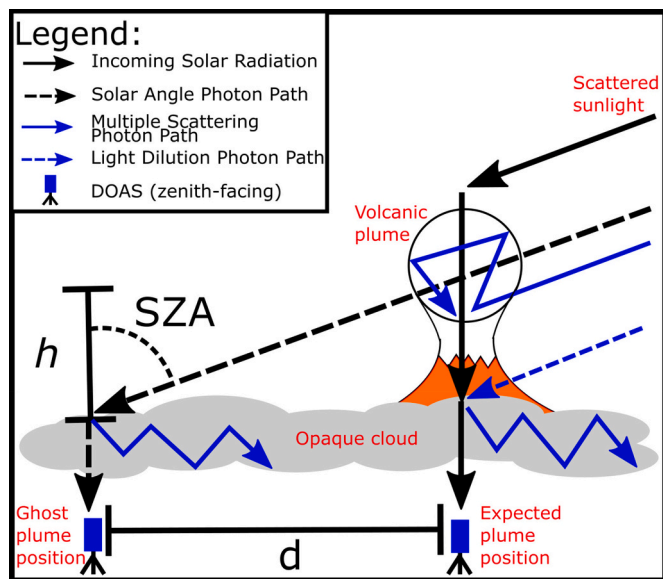
Fig. 1. Ghost plume mechanism with an assumed ideal photon pathway from the direct solar beam that crosses the plume and gets scattered down by single scattering in a cloud below the plume toward the Differential Optical Absorption Spectroscopy (DOAS) telescope. The key parameters are the solar zenith angle (SZA); the altitude difference between the plume and a lower layer of clouds (*h*); and the offset-distance (*d*) where the ghost plume is observed.

to test the influence of factors such as SZA, cloud height, plume height, cloud layer thickness, cloud aerosol optical depth (AOD), and plume AOD on the derived SO_2 cross-sectional burdens. AOD is defined analogous to the trace gas optical depth (Eq. (3)) as the integral of the aerosol extinction coefficient ε over the light path.

$$AOD = -log\left(\frac{I}{I_0}\right) = \int_{0}^{L} \varepsilon \bullet dx \qquad (5)$$

Eq. (5) considers a narrow beam of light passing through an aerosol cloud. Extinction of the initial intensity I_0 occurs solely by aerosol scattering or absorption. An AOD of 0 describes an aerosol-free region of the atmosphere. An AOD of 1 represents a situation in which 63% of photons are scattered or absorbed on aerosols on their path through the cloud. Plumes with AODs of ~4 or greater are completely opaque such that a black object behind the plume can no longer be discerned (Koschmieder, 1925). In our model study, we adjusted the AOD between 0 (aerosol-free) and 20 (practically all photons are scattered on aerosols) to examine various levels of plume opacity.

We compare cross-sectional burdens of simulated traverses to those calculated assuming ideal radiative transfer, i.e., all photons passing vertically through the plume. These results provide guidelines for evaluating zenith-facing mobile DOAS results under similar conditions to make the best use of available data within a reasonable uncertainty threshold. Herein, we somewhat arbitrarily define a cross-sectional burden within ±25% of the true value as a "reasonable" uncertainty. Notably, the true acceptability of a measurement is dependent on user needs. In the case of monitoring volcanic gas for large-scale changes (an increase from 100's to 1000's of t day^{-1} SO_2) then a larger uncertainty in measurements may be acceptable. Additionally, we only consider error to cross-sectional burden; however, misattribution of a ghost plume as the main plume under high AOD conditions can result in unassessed errors to measurement geometry and wind speed should an emission rate calculation be attempted.

2.1. Model constraints

We simulate zenith-facing mobile DOAS traverses using the McArtim radiative transfer model (Deutschmann et al., 2011) to test the effects of the specified parameters (Table 1) on the modeled SO_2 cross-sectional burden. McArtim is a 3-dimensional backward Monte Carlo radiative transfer model. It uses back-propagation to simulate photon paths from the instrument to the sun through Earth's atmosphere, specified by different atmospheric compositional profiles (e.g., gas molecules, clouds, and aerosol particles) with different scattering and absorption properties. We conducted 217 different model permutations that vary cloud layer thickness (200, 400, 800 m), SZA (1, 30, 60), plume AOD (0, 1, 4, 8), and cloud AOD (0, 1, 2, 4, 8, 20) to test the influence of only these variables on the resulting plume SO_2 cross-sectional burden (see Table 1). So that the modeled traverses are comparable, each simulation assumes: (a) a cylindrical horizontal plume with constant diameter of 400 m, centered at 1600 m altitude, containing a uniform SO_2 mixing ratio of 250 parts per billion (ppb) corresponding to a vertical column density through the plume center of 2.5×10^{17} molec cm^{-2}, and (b) a rectangular aerosol cloud layer below the plume with infinite length and variable thickness (Table 1), centered at 400 m elevation and containing no SO_2. We simulate 10^5 photon trajectories through our model atmosphere. The SO_2 concentration is integrated along the path of each individual photon. The simulated column density is then determined by weighing each path-integral with the likelihood of that path and taking the weighted average. Simulating 10^5 photons reduces the uncertainty in modeled path integrals to less than 10%. By moving the horizontal position of our zenith-facing instrument, we model the SO_2 column density at each measurement location within a simulated mobile DOAS traverse. A traverse consists of simulated SO_2 column density measurements made perpendicular to plume direction at 50 m increments, from −3000 m to +2000 m horizontal positions below the center of the simulated plume. The relative azimuth of the sun is chosen to be perpendicular to the plume for simplified geometric predictions of ghost plume location, where a non-perpendicular azimuth of the sun relative to the plume may cause a ghost plume manifestation closer to the plume. The traverse length is asymmetrical (1000 m longer on one side) to account for the expected manifestation of the ghost plume on the side farthest from the sun. Each simulated DOAS retrieval is conducted at a wavelength of 315 nm, which was selected to describe absorption from a typical DOAS fit window for SO_2 (Kern et al., 2010). Fixed instrument parameters during each simulation were an instrument altitude of 0 m and an instrument field of view of 0.3°. Fixed atmospheric parameters during each simulation were a plume single scattering albedo of 0.9 to represent some absorption of photons by ash along with a Henyey-Greenstein asymmetry factor of 0.8; a cloud single scattering albedo of 1 is used to represent perfect scattering along with an asymmetry factor of 0.8 (Chandrasekhar, 1950). A ground albedo of 0.03 is used to represent water (Trlica et al., 2017).

2.2. Plume selection criteria for determining cross-sectional burdens

All DOAS measurements initially determine the column density along an effective light path of the measured photons. In zenith-facing mobile DOAS measurements of volcanic plumes, it is common to assume that the effective light path, or the slant column density (SCD), is

Table 1
Model parameter values used in this study, including the range of cloud and plume aerosol optical depth (AOD) values.

Parameter	Values Used					
Cloud layer thickness [m]	200	400	800			
SZA [°]	1	30	60			
Plume AOD	0	1	4	8		
Cloud AOD	0	1	2	4	8	20

equal to a straight vertical line through the plume, the so-called vertical column density (VCD). Although this approximation can fail for opaque plumes or cloudy atmospheric conditions, as we will discuss here, it is an acceptable assumption for optimal viewing conditions and transparent plumes (Kern et al., 2010). The standard approach to calculate plume SO_2 cross-sectional burden (molec m^{-1}) is to integrate the area under the SO_2 SCD profile for each traverse. These integrated areas require defining (1) the plume limits, or the X (location) values where the plume profile transitions from background to plume and plume to background, and (2) the plume baseline, or the minimum SO_2 SCD value representative of background conditions. Both parameters present an opportunity to have user-induced bias that can contribute to measurement uncertainties.

Notably, in real-world scenarios the initial light intensity, I_0, when used as a reference spectra assumes that there is not any SO_2 along the optical path. Thus, the selection of spectra for I_0 which contain some degree of SO_2 may produce a "SO_2 contaminated reference spectra," effectively producing a lower SCD value in all other analyzed spectra (Eq. (3)). One method to solve for these problems in SO_2 contaminated datasets is to perform a "baseline correction" by adding or subtracting the same column density to all points within a dataset. Our process of defining the plume limits and performing a baseline correction is analogous to this process.

To prevent this bias, we define some criteria to allow plume baseline and limit parameters to be calculated consistently and automatically (Fig. 2A). To identify plume limits, we first calculate a moving mean SO_2 SCD for 5 adjacent pixels to minimize noise. We then identify plume limits as the derivative of the SO_2 SCD along horizontal position ($\frac{dSCD}{dx}$; Fig. 2B), where the plume start and end are defined as the first and last $\frac{dSCD}{dx}$ value above and below a threshold value. We select -1×10^{13} (molec cm^{-3}) as our $\frac{dSCD}{dx}$ plume limit threshold because it is sensitive enough to capture plume boundaries without being too sensitive to changes in SCD due to background noise. The minimum SCD value between the plume limits is then selected as the plume baseline and subtracted from all other SCD values. The simulated cross-sectional burden, or the integrated area beneath the curve, is then compared to the theoretical cross-sectional burden of the plume to assess accuracy, where the theoretical cross-sectional burden (CSB) may be calculated as Eq. (6):

Fig. 2. Illustration of baseline and plume limit selection method. (Top) Example traverse with points inside the limits of plume selection in green and points excluded in red. (Bottom) Plume baseline and limits related to the $\frac{dSCD}{dx}$ threshold, where the plume edges are defined as the first value over 1×10^{13} (molec cm^{-3}) and the last value under -1×10^{13} (molec cm^{-3}). (For interpretation of the references to colour in this figure legend, the reader is referred to the web version of this article.)

$$CSB_{theoretical} = \frac{\pi}{4} \times C_{SO_2} \times d_{plume}^2 \qquad (6)$$

with both the SO_2 concentration ($C_{SO2} = 6.25 \times 10^{12}$ molec cm^{-3}–250 ppb) and the plume diameter ($d_{plume} = 400$ m) being known model input parameters.

Based on the modeled traverses, our method of cross-sectional burden analysis is not sensitive to changes in threshold values. Different threshold values for $\frac{dSCD}{dx}$ of the same magnitude do not appear to produce large deviations in measured cross-sectional burden, generally within ±10%. We do find that the largest sensitivity related to our method to be a function of baseline correction, where non-baseline corrected measurements are generally greater than their baseline corrected counterparts, in extreme cases up to 100% larger. These discrepancies in cross-sectional burden demonstrate the influence of SO_2 contamination. For real-world measurements performed under cloudy conditions, spectra collected many kilometers away from the plume can still be contaminated and baseline adjustments will need to be considered. Our method of selecting the baseline by rate of change provides a standardized way to accomplish this.

3. Results

3.1. Modeled traverses

Based on our model runs, we find that increasing cloud and plume AOD cause a general broadening and decrease in the amplitude of the SCD curve, and for SZA >1° lead to the formation of horizontally offset ghost plumes. These results are illustrated by six scenarios depicted in Figs. 3A–F. The scenarios vary by increasing SZA from 1° (0° is avoided to avoid aiming the instrument directly at the sun), 30°, and 60° as we model zenith-facing observations for different latitudes and times of the day, with the left column representing a transparent plume (AOD = 0) and the right column representing an opaque plume (AOD = 4). In the following, we refer to plumes and clouds as transparent (AOD = 0), semi-transparent (0 < AOD < 4) and opaque (AOD ≥ 4). Examples are shown for a 400 m thick cloud in each scenario, with cloud AOD varying from 0 to 20. Detailed observations for each scenario are described below.

3.1.1. Scenario a (Transparent plume, SZA = 1°)

The simplest model scenario—a transparent plume with the sun overhead—demonstrates that increasing cloud opacity results in plumes appearing substantially broader (Fig. 3A). In this case we have a SZA = 1°, representing photons supplied from a nearly directly overhead source, and a transparent plume (AOD = 0). In each scenario the simulated SO_2 SCD curve is shown as a function of cloud AOD, which varies from 0 (transparent cloud) to 20 (opaque cloud). In the case of a transparent cloud (AOD = 0) the simulated measurements match the input plume SO_2 VCD versus position curve in shape and amplitude, with a plume width of ~400 m and a maximum SCD of 2.37×10^{17} molec cm^{-2} at the plume center. Increasing cloud AOD produces a broadening (negative kurtosis) of the plume SCD curve. At lower cloud AOD values (1–4), this broadening is generally gradual and has minimal effect on the apparent plume width or maximum SCD. Transitioning to higher cloud AOD scenarios (> 4), the peak broadening effect increases, resulting in measured plumes >2 km wider than the actual plume and maximum SO_2 SCDs < 40% of actual VCD values.

The observed variation in SO_2 cross-sectional burden error with respect to the theoretical model as a function of increasing cloud AOD (Fig. 4A) shows that a condensed lower cloud alone will produce an acceptable cross-section. The integrated cross-sectional burden from a case with both a transparent plume and cloud (e.g., Scenario A, Fig. 3A) is 95% of the expected value. Increasing cloud AOD values to > 1 leads to increasing underestimations of the overall cross-sectional burden
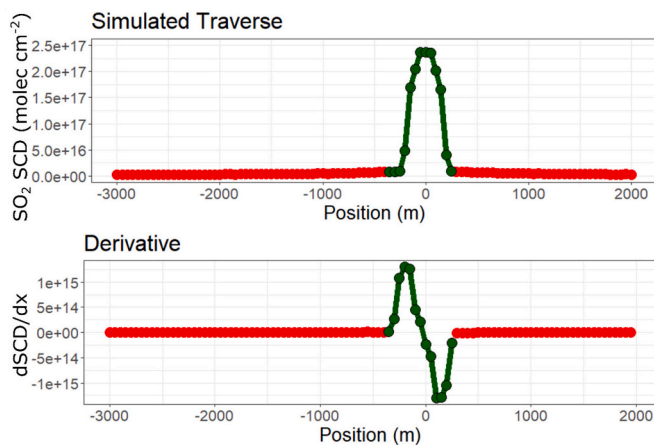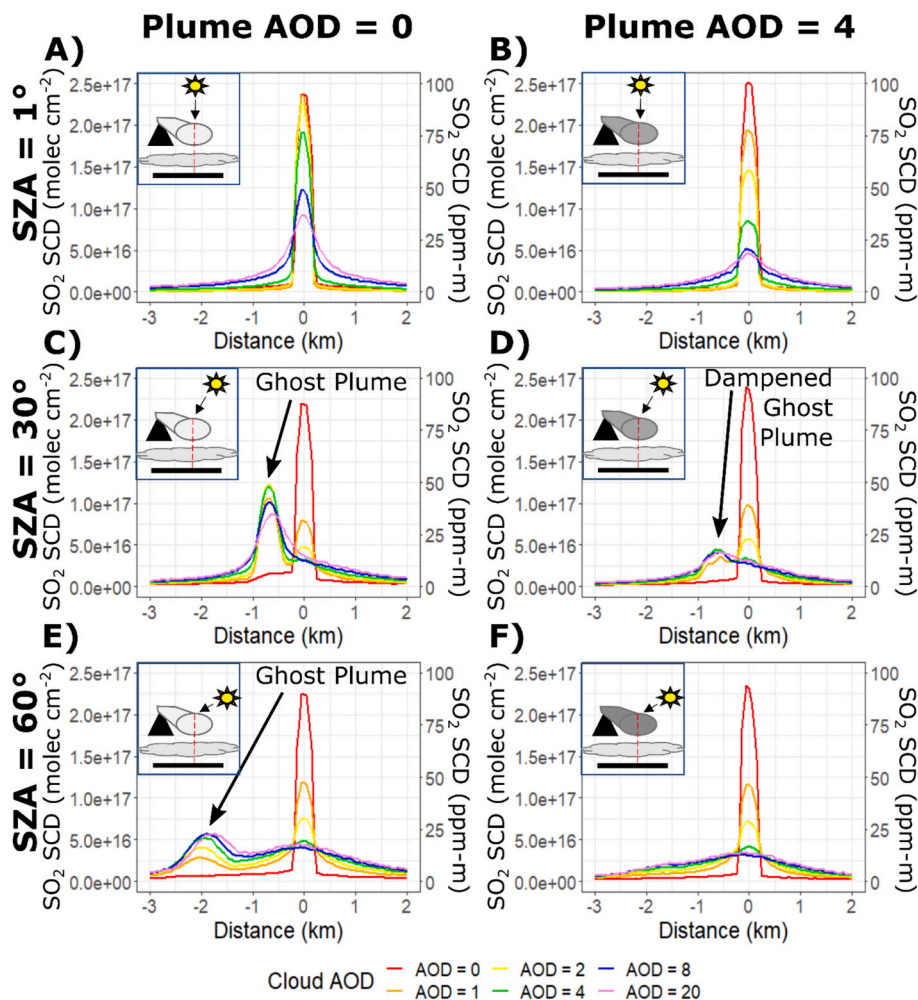
Fig. 3. Simulated Differential Optical Absorption Spectroscopy (DOAS) traverses for a 400 m diameter SO_2 plume with a central SO_2 vertical column density (VCD) of 2.5×10^{17} molec cm^{-2} (100 ppm•m). A 400 m thick cloud is located between the plume and the telescope. Traverses demonstrate two plume aerosol optical depth (AOD) conditions: transparent (AOD = 0; left column) and opaque (AOD = 4; right column), and three solar zenith angles (SZA) (top: SZA = 1°; middle: SZA = 30°; bottom: SZA = 60°). The red line in all panels represents simulated traverse results for a transparent cloud that accurately depicts the plume location. Increased SZA results in a peak SO_2 slant column density (SCD) displaced horizontally by ~700 m from the true location for a SZA of 30° and by ~2050 m for a SZA of 60°. Increased plume AOD results in an attenuation of the ghost plume effect such that it is barely perceptible for SZA = 60°, AOD = 4 scenarios. (For interpretation of the references to colour in this figure legend, the reader is referred to the web version of this article.)

until cloud AOD values of > 8, after which the cross-sectional burden trends back towards the expected value. In all cases for this scenario (transparent plume and near-vertical SZA), SO_2 cross-sectional burdens are within 27% of the expected value and the majority are within 10% of the expected value.

3.1.2. Scenario B (Opaque plume, vertical SZA)

Increasing plume opacity in our model decreased the maximum measured column density. In this case we observe an immediate and rapid dampening of the plume maximum SO_2 SCD with even slight increases in cloud opacity (Fig. 3B); in comparison to that of a transparent plume (AOD = 0), the maximum SCD is reduced by ~20% for a semi-transparent cloud with AOD = 1 and up to 82% for an opaque cloud with AOD = 20. In this scenario the shape of the plume SCD curve also appears to be more rounded (negatively kurtosed) than its transparent counterpart (Scenario A), resulting in slightly broader profiles across all traverses where cloud AOD > 1.

Errors in plume cross-sectional burden (Fig. 4A) vary as a function of cloud opacity and follow similar trends to scenario A (Fig. 4A). Initial cross-sectional burden for transparent cloud scenarios are 103% of the theoretical value and decrease rapidly to a minimum of 38% of the theoretical value at a cloud AOD = 8. At cloud AOD values > 8, SO_2

cross-sectional burdens begins to trend upward slightly. In the case of an opaque plume, cross-sectional burdens exceed errors of 25% of the theoretical value for cloud AOD > 1.

3.1.3. Scenario C (Transparent plume, SZA = 30°)

Non-zenith solar angles are found to not only result in broader apparent plumes, but also the emergency of a secondary apparent plume. First, with the cloud AOD = 0 traverse we find that an aspect of skewness, or tailing, is introduced into the SCD curve away from the direction of the sun. This tail manifests as an area of higher-than-background SCD extending approximately 1 km away from the plume center (Fig. 3C), suggesting the hint of a ghost plume. At all nonzero cloud AOD values we model apparent ghost plumes where a portion of the plume SO_2 SCD is spatially offset from its expected location, with a local SCD maximum at ~700 m. At cloud AOD values of 1–2, our models indicate a rapid decrease in maximum SO_2 SCD to < 40% of the value for a transparent cloud (Fig. 3C) at the expected location. In conjunction with the rapid SCD decrease at the expected location, SCD rapidly increases under the ghost plume location leading to two local SCD maxima. Increasing cloud AOD > 4 results in the disappearance of the peak at the actual plume location and its replacement with a single SO_2 maximum value in the geometrically offset (ghost-plume) location.
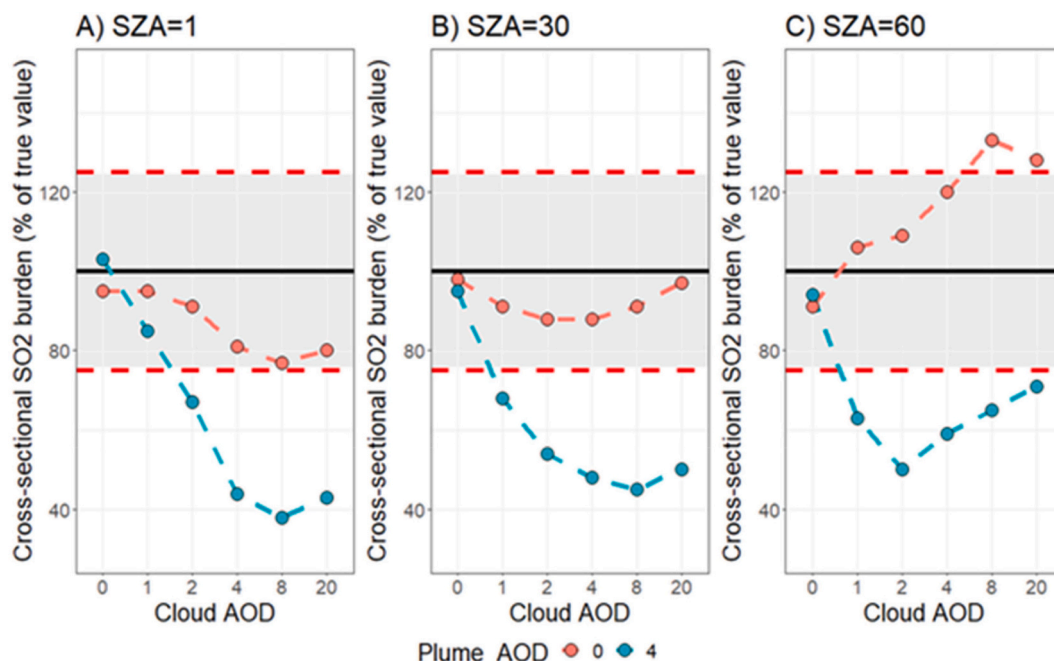
Fig. 4. Error in SO_2 cross-sectional burden associated with the six scenarios shown in Fig. 3. SO_2 cross-sectional burden is expressed as a % of the theoretical value (black horizontal line). Discrepancies of $\pm 25\%$ are indicated by red dashed horizontal lines. The three panels depict simulations for solar zenith angle (SZA) = 1° (left), SZA = 30° (center), and SZA = 60° (right) under differing cloud aerosol optical depth (AOD) conditions (x-axis). Cross-sectional burden from transparent plumes (red points) are generally within the accepted confidence interval whereas cross-sectional burden from traverses with opaque plumes (blue points) are more substantially underestimated. (For interpretation of the references to color in this figure legend, the reader is referred to the web version of this article.)

Similar to scenario A, we find that traverses modeled under higher cloud AOD values lead to broader SO_2 SCD peaks.

Despite the ghost plume phenomena, all cross-sectional burdens under scenario C (Fig. 4B) fall within 12% of the actual value, regardless of cloud AOD. Transparent plume model results for these conditions give SO_2 burdens equal to 98% of the true value, the closest of all iterations considered for this study. A minimum cross-sectional burden of 88% of the theoretical value is achieved at a cloud AOD = 2. The SO_2 cross-sectional burden increases to 97% of theoretical at cloud AOD = 20. Patterns observed in this scenario are similar to those under scenario A; however, cross-sectional burdens begin to increase again at a lower degree of cloud opacity around AOD values of 2–4 (Fig. 4B).

3.1.4. Scenario D (Opaque plume, SZA = 30°)

With an opaque volcanic plume and sufficiently condensed lower cloud layer, ghost pume effects are somewhat dampened. In this case we still observe a ghost plume, but the magnitude of the plume SO_2 SCD is notably dampened in comparison to scenario C. During opaque cloud conditions (AOD ≥ 4), a single peak is present with the maximum SCD manifesting ~700 m from the actual plume position with the direction of tailing toward the sun (Fig. 3D). At cloud AOD ≤ 2 values, the maximum SCD beneath the actual plume location is larger than in scenario C (transparent plume).

SO_2 cross-sectional burden for scenario D is underestimated with respect to theoretical for all cloud AOD conditions. With increasing cloud AOD there is a precipitous decline in SO_2 cross-sectional burden to a minimum of 44% of the theoretical value at a cloud AOD of 8. At cloud AOD values >8, our estimates of the cross-sectional burden are slightly less underestimated, at 50% of the theoretical value. For this scenario of an opaque plume and SZA = 30° (Fig. 4B), only a transparent cloud (AOD = 0) achieves an uncertainty within $\pm 25\%$ of the true value.

3.1.5. Scenario E (Transparent plume, SZA = 60°)

Increased solar zenith angles result in the emergence of a ghost plume farther away from the main volcanic plume. Many aspects of

these traverses are similar to scenario C though slightly more exaggerated. In conditions of a transparent plume and cloud AOD ≥ 1, we observe a ghost plume 2 km from the expected plume location and a broad tailing in the SO_2 SCD curve several kilometers farther away from the sun (Fig. 3E). Increasing cloud opacity (cloud AOD > 1) leads to a rapid decline in SO_2 SCD to < 50% of the value for no clouds and the emergence of a ghost plume. In contrast to scenario C, cloud AOD values ≥ 4 do not appear to entirely obfuscate the plume SO_2 peak beneath its expected location, instead showing one peak at the ghost plume location and one broad, heavily kurtic, peak beneath the expected location.

Unlike the previous scenarios that largely underestimate the plume SO_2 cross-sectional burden, scenario E shows an SO_2 plume cross-sectional burden overestimated with respect to actual in all cases except for a cloud AOD = 0. We observe a minimum SO_2 cross-sectional burden of 90% of the true value in ideal atmospheric conditions (cloud AOD = 0; Fig. 4C), and a maximum (overestimation) of 133% of the true value for an opaque cloud (cloud AOD = 8). This scenario also shows the greatest variability in SO_2 cross-sectional burden (43%) of the three transparent plume scenarios.

3.1.6. Scenario F (Opaque plume, SZA = 60°)

Condensed volcanic pllumes, when modeled with a condensed lower cloud layer and high solar zenith angle, rapidly begin to produce a single broad apparent plume. For cloud AOD = 0 conditions, the plume appears in its expected location with no apparent tail or ghost plume effect seen. As cloud opacity increases (cloud AOD ≥ 1) the SO_2 SCD curve appears in all cases to be a single heavily kurtic and slightly skewed peak. Curve skewness and kurtosis both increase with increasing cloud AOD and in no case is there a clear secondary ghost plume peak. Instead, in cloud AOD ≥ 4 scenarios, we model a single SO_2 peak with a maximum SCD approximately beneath the expected plume location extending in width over ~5 km, or ~4.5 km wider than theoretical.

The modeled SO_2 cross-sectional burden for scenario F is underestimated with respect to theoretical in all cases (Fig. 4C). This underestimation increases to 50% of the true value as cloud opacity increases

from an AOD of 0 to 2. For cloud AOD > 2 conditions the underestimation decreases, reaching 71% of the true value. As in scenario E, only the cloud AOD = 0 case of scenario F yields an SO_2 cross-sectional burden within an acceptable uncertainty of $\pm 25\%$.

3.1.7. Additional scenarios

General observations made for the 400-m-thick cloud scenarios discussed above are broadly consistent with model runs performed for other cloud thicknesses and are not discussed in detail here. Thicker clouds of 800 m and thinner clouds of 200 m (Appendices A, B) do not produce appreciable deviations in observed peak shapes relative to the 400-m-thick cloud scenarios, with the few exceptions being those scenarios with substantial amounts of multiple scattering such as for 800-m-thick clouds and cloud AOD > 8.

We also explored the effects of plume AOD between 0 and 8 on the uncertainty in derived SO_2 cross-sectional burdens. Unlike cloud thickness, different plume AOD values have a more substantial effect on cross-sectional burden uncertainty, as demonstrated in Fig. 4 considering differences between a plume AOD of 0 and 4 and as found in previous studies (Kern et al., 2010; Kern et al., 2012). We find that a plume AOD of 1 (a semi-transparent plume) leads to a cross-sectional burden underestimation 1–15% lower than corresponding transparent plume (AOD = 0) scenarios. We also find that cross-sectional burdens under a heavily opaque plume (AOD = 8) are consistently lower than plume AOD = 4 scenarios, with uncertainties regularly exceeding 50% of theoretical.

4. Discussion

4.1. Model results and errors in cross-sectional burden retrievals

Full error estimates in the construction of SO_2 emission rates consist of uncertainties in several broad categories including wind speed, instrument error, measurement geometry, and atmospheric scattering (Galle et al., 2010). Both atmospheric scattering and wind speed are identified as large components of error in total SO_2 emission rate calculations. Our model results indicate that relatively accurate SO_2 emission rate measurements may be acquired for (semi-) transparent plumes (AOD $\leq$ 1) even when clouds are present between the plume and the instrument. Even though the maximum measured SCD decreases beneath the plume with increasing cloud opacity, thickness, and SZA (Fig. 3), the resulting peak broadening for transparent plumes still leads to cross-sectional burdens that agree within $\pm 25\%$ of the theoretical value in most cases (Fig. 4). Furthermore, we show that while there may initially be a decrease in cross-sectional burdens with increasing cloud AOD, peak broadening eventually leads to larger cross-sectional burdens that again approach the theoretical value (Fig. 4). This suggests that if the overhead volcanic plume is sufficiently transparent, non-ideal atmospheric conditions due to low cloud presence generally create errors in cross-sectional burden of only $\leq$ 25%. Our results also indicate that the location of ghost plumes can be predicted quite accurately from simple geometrical considerations of the position of the sun and difference in altitude between the plume and underlying cloud. For the scenarios considered we found ghost-plume peaks displaced laterally by ~700 and ~2000 m opposite from the sun position for SZA of 30° and 60°. These model results agree well with the predictions from Eq. (4). In real-world scenarios, where suspected ghost plumes exist as two distinct peaks during a zenith-facing mobile DOAS traverse, all the required parameters should be measurable to approximate the altitude of a plume above a cloud layer.

Scenarios B, D, and F with an opaque plume (plume AOD = 4) show a substantial underestimate of the cross-sectional burden and demonstrate that atmospheric scattering is a large contributor to error in emission rate measurements under opaque plume and low cloud conditions (Fig. 4). It is well-understood that light dilution can lead to underestimates of plume SCDs for opaque plumes, even in the absence of

low-cloud conditions (Kern et al., 2010). We provide increased context in this study about the effect of radiative transfer from opaque plumes on derived cross-sectional burdens. Due to the complex nature of multiple scattering, speculation about the physical interpretation of each individual measurement in this model is difficult to describe in detail. However, we observe the compound effect of several scattering events, which are contingent upon specific measurement conditions. Scenarios A, C, and E still find that conditions with a transparent plume and opaque cloud between the plume and the DOAS telescope yield acceptable uncertainties (within $\pm 25\%$ for all scenarios but one). This indicates that zenith-facing mobile DOAS measurements can be collected under low-cloud conditions yet produce informative emission rate results. Our results indicate that opaque low clouds by themselves are not a large contributor to total SO_2 emission rate error and that definitions of poor atmospheric measurement conditions can be narrowed to include only those with an opaque plume.

Determining plume transparency when the plume is obscured by low clouds is rarely possible and requires external resources such as fortuitously located webcams or observer/pilot reports. Misidentifying a ghost plume as the true plume location can lead to errors in measurement geometry that further increase the total error in SO_2 emission rate. In scenarios where two plumes are registered on a zenith-facing mobile DOAS traverse, knowledge of solar position provides information on which plume is most likely in the correct position. All scenarios examined in our models where the sun is not directly overhead in conjunction with an opaque cloud layer between the DOAS instrument and plume cause modification of plume cross-sectional shape, and most lead to ghost-plume emergence. Ghost plumes are seen even at low cloud AODs of 1 in thinner cloud layers (200 m; Appendix A), which indicates that plume shape modification can begin to occur under many commonly occurring real-world situations. These low cloud AOD scenarios are common in otherwise optimal urban and marine conditions, where low-lying haze or aerosolized sea salt can generate ambient AOD values of 0.1–0.4 at the wavelengths considered for DOAS retrievals of SO_2 (Mulcahy et al., 2009). Examples of marine volcanoes include the Aleutian Islands in Alaska.

In general, the model studies show that the maximum detected SO_2 column density decreases in the presence of a cloud layer beneath the plume, whereas the width of the detected plume increases. For weak plumes, this can lead to a larger fraction of measurements along a traverse registering below the detection limit of the utilized instrument. This can lead to underestimates of the cross-sectional burden beyond what is presented in our model results, but a quantitative assessment is beyond the scope of this study as it depends on the sensitivity of the instrument utilized in the measurements.

4.2. Implications for Plume Measurement Methodology

Considering our model results, the following practices can enhance accurately collecting zenith-facing mobile DOAS measurements of volcanic SO_2 emission rates for volcano monitoring. First, error can be minimized by ensuring that measurements are collected downwind from the vent where the plume is more likely to be more transparent, and thus less prone to large scale underestimation (Fig. 4). Measurements with a low cloud layer and transparent plume can be increasingly common farther from the volcanic edifice as the plume dilutes in the atmosphere, generally at distances of at least 1 km (Matsushima and Shinohara, 2006). Secondly, extending zenith-facing mobile DOAS traverses recorded with low cloud cover beyond any SO_2 signals for several km in the direction opposite to the solar position can capture a potential ghost plumes. For example, in our scenario of a plume ~1 km above the cloud layer, extending the traverse up to 1–2 additional kilometers properly captured background conditions and observed ghost plumes. In the case of conditions with clouds scattered beneath the plume, extending the traverse can provide an opportunity to visually constrain overlying plume conditions if low clouds are localized. Notably, in scenarios where

there are localized clouds directly beneath the plume but not in a favorable placement for ghost plume emergence, a ghost plume cannot be measured and the cross-sectional burden can be substantially underestimated. To ascertain the degree of plume opacity while the sun is visible, complementary use of a photometer (e.g., Barreto et al., 2016) can be employed during traverses to quantify AOD. Without specialized equipment, acquisition of complementary visual observations through webcam or uncrewed aircraft systems (drone) imagery can be used to approximately constrain plume AOD and estimate emission rate uncertainties. If no resources exist to confirm the opacity of the plume during the traverse, the range of scenarios presented here (Fig. 3) can also be used as a guide to ascribe a level of uncertainty (Fig. 4) to a range of overlying atmospheric and plume conditions (see Appendix C). Thirdly, judgment of the shape of the plume and the detection of a plume in an unexpected location relative to the location of the sensor, plume, and sun can be used to determine if a ghost plume is or is not present.

4.2.1. Automation of plume detection

As discussed above, selecting plume horizontal limits and SO_2 baseline values is somewhat subjective and analysts use different guidelines to make these choices that ultimately affect the derived SO_2 cross-sectional burden and emission rates. Our modeling study shows that, if we simply integrate the SO_2 SCD along the entire traverse, we obtain approximately a 10% overestimate of the SO_2 cross-sectional burden for optimal atmospheric conditions (transparent plume, no clouds) due to an uncertain background. We hypothesize that this is mostly caused by photons that pass through the plume and are then scattered beneath it toward the instrument. These photons carry the absorption signature of SO_2 in the plume but, depending on the SZA, are detected away from the plume and lead to a slightly overestimated cross-sectional burden. This effect is analogous to, but less pronounced than, the ghost plume effect and occurs even in cloud-free conditions due to scattering on air molecules rather than cloud droplets.

If we apply the plume selection criteria we introduced above, the SO_2 column densities along a traverse are adjusted for a small but non-zero baseline SO_2 SCD (typically in the range of 2–4×10^{15} molec cm^{-2} during optimal conditions). Low cloud conditions with moderate to high (≥ 4) AOD can further increase the automatically derived baseline SCD to 6–11×10^{15} molec cm^{-2} due to multiple scattering within the cloud layer, causing a further broadening of the measured plume SCD peak. Using our SCD derivative method to automatically define the plume limits can help properly identify a reasonable background SCD value and plume extent. Our results show that calculated cross-sectional burdens are within reasonable margins ($\pm 25\%$) of the theoretical value. In our analyses without an adjusted baseline under high cloud AOD and SZA scenarios, the cross-sectional burden was overestimated by as much as 100% (Appendix B). Secondly, as SZA increases, skewness is introduced such that the plume is no longer symmetrical on each side. At high SZA values in optimal atmospheric conditions, the degree of skewness increases such that the background SCD appears higher several kilometers beyond the plume on the side opposite the solar position. Because of the nature of these shapes, $\sim 10\%$ error was found in our ideal traverse cross-sectional burdens with the thresholds and averaging that we selected for baseline determination.

The challenge of manually selecting an appropriate baseline and manually defining plume limits introduces user-induced error in SO_2 emission rate calculations depending on the criteria used for cross-sectional burden determination that can be minimized through the automated method presented here. For a plume input SO_2 VCD of 2.5×10^{17} molec cm^{-2} at plume center, a $\frac{dSCD}{dx}$ threshold of 1×10^{13} molec cm^{-3} to determine plume limits was found to be sensitive enough to accurately capture small features considered part of the plume or ghost plume while not capturing noise. Additionally, averaging 5 consecutive SO_2 column measurements was found to reduce the model photon noise to below 1×10^{13} molec cm^{-3} even for the extreme scenarios (e.g., cloud

AOD = 20, scenario F). Other threshold values may be more appropriate for differing sets of real-world data depending on the atmospheric concentration of SO_2 and signal/noise ratio achieved during the respective measurement. Because the $\frac{dSCD}{dx}$ threshold value of 1×10^{13} molec cm^{-3} may not hold true across all real-world measurements, more relevant site-specific criteria based on SO_2 emission rate and level of volcanic activity can be developed and utilized.

5. Conclusions

The emergence of ghost plumes is a known, but until now relatively poorly studied, phenomenon in remote sensing of volcanic SO_2 plumes. Although it is commonly accepted that different atmospheric conditions can affect SO_2 column density retrievals from Differential Optical Absorption Spectroscopy (DOAS) measurements, we have expanded the current body of knowledge to constrain the influence of solar zenith angle and below-plume cloud aerosol optical depth (AOD) on SO_2 column density measurements. We have presented a visual and quantitative guide for how different low-cloud atmospheric conditions modify plume shapes and generate ghost plumes in zenith-facing mobile DOAS traverses. Furthermore, we have demonstrated that for SO_2 column densities commonly measured during persistent degassing ($\sim 2.5 \times 10^{17}$ molec cm^{-2} SO_2), a below-plume cloud will modify the shape of a plume slant column density (SCD) profile along the traverse, but that the resulting cross-sectional burden will generally agree within $\pm 25\%$ of the input value if the plume is relatively transparent (AOD < 1). Our research demonstrates an application of the McArtim model to simulate DOAS traverses of simple volcanic plumes; however, due to the complex nature of real-world plumes, such simulations may not perfectly match real-world observations. We have also shown that modification of plume shapes due to low clouds may be more common than previously thought. Our findings indicate that zenith-facing mobile DOAS traverse measurements made under suboptimal atmospheric conditions with haze, fog, or low-lying clouds can still yield relatively accurate SO_2 emission rate measurements for volcano monitoring purposes.

CRediT authorship contribution statement

D. Skye Kushner: Writing – original draft, Visualization, Investigation, Formal analysis, Conceptualization. **Taryn Lopez:** Writing – review & editing, Supervision, Project administration, Methodology, Funding acquisition, Conceptualization. **Christoph Kern:** Writing – review & editing, Visualization, Supervision, Software, Methodology, Formal analysis, Conceptualization. **Santiago Arellano:** Writing – review & editing, Formal analysis, Data curation. **Nemesio M. Pérez:** Data curation. **José Barrancos:** Data curation.

Declaration of competing interest

David Skye Kushner reports financial support was provided by the U.S. Geological Survey. Santiago Arellano reports financial support was provided by the Swedish National Space Board. The other authors declare that they have no known competing financial interests or personal relationships that could have appeared to influence the work reported in this paper.

Data availability

All data, including full model output files, are included in the appendices to this paper.

Acknowledgments

We would like to thank Bo Galle, William Simpson, and two anonymous reviewers for constructive feedback on this manuscript.

Appendix. Supplementary data

Supplementary data to this article can be found online at https://doi.org/10.1016/j.jvolgeores.2024.108217.

References

Arellano, S., Galle, B., Apaza, F., Avard, G., Barrington, C., Bobrowski, N., Bucarey, C., Burbano, V., Burton, M., Chacón, Z., Chigna, G., Clarito, C.J., Conde, V., Costa, F., De Moor, M., Delgado-Granados, H., Di Muro, A., Fernandez, D., Garzón, G., Gunawan, H., Haerani, N., Hansteen, T.H., Hidalgo, S., Inguaggiato, S., Johansson, M., Kern, C., Kihlman, M., Kowalski, P., Masias, P., Montalvo, F., Möller, J., Platt, U., Rivera, C., Saballos, A., Salerno, G., Taisne, B., Vásconez, F., Velásquez, G., Vita, F., Yalire, M., 2021. Synoptic analysis of a decade of daily measurements of SO_2 emission in the troposphere from volcanoes of the global ground-based Network for Observation of Volcanic and Atmospheric Change. Earth Syst. Sci. Data 13, 1167–1188. https://doi.org/10.5194/essd-13-1167-2021.
Barreto, Á., Cuevas, E., Granados-Muñoz, M.-J., Alados-Arboledas, L., Romero, P.M., Gröbner, J., Kouremeti, N., Almansa, A.F., Stone, T., Toledano, C., Román, R., Sorokin, M., Holben, B., Canini, M., Yela, M., 2016. The new sun-sky-lunar Cimel CE318-T multiband photometer – a comprehensive performance evaluation. Atmos. Meas. Tech. 9, 631–654. https://doi.org/10.5194/amt-9-631-2016.
Chandrasekhar, S., 1950. Radiative Transfer. Oxford Press, Oxford.
Deutschmann, T., Beirle, S., Frieß, U., Grzegorski, M., Kern, C., Kritten, L., Platt, U., Prados-Román, C., Puķite, J., Wagner, T., Werner, B., Pfeilsticker, K., 2011. The Monte Carlo atmospheric radiative transfer model McArtim: Introduction and validation of Jacobians and 3D features. J. Quant. Spectrocs. Ra 112 (6), 1119–1137. https://doi.org/10.1016/j.jqsrt.2010.12.009.
Edmonds, M., Herd, R.A., Galle, B., Oppenheimer, C.M., 2003. Automated, high time resolution measurements of SO_2 flux at Soufrière Hills Volcano. Montserrat B Volc 65 (8), 578–586. https://doi.org/10.1007/s00445-003-0286-x.
Fischer, T.P., Roggensack, K., Kyle, P.R., 2002. Open and almost shut case for explosive eruptions: Vent processes determined by SO_2 emission rates at Karymsky volcano, Kamchatka. Geology 30 (12), 1059–1062. https://doi.org/10.1130/0091-7613(2002)030<1059:OAASCF>2.0.CO;2.
Galle, B., Oppenheimer, C., Geyer, A., McGonigle, A.J.S., Edmonds, M., Horrocks, L., 2003. A miniaturised ultraviolet spectrometer for remote sensing of SO_2 fluxes: a new tool for volcano surveillance. J. Volcanol. Geotherm. Res. 119 (1–4), 241–254. https://doi.org/10.1016/S0377-0273(02)00356-6.
Galle, B., Johansson, M., Rivera, C., Zhang, Y., Kihlman, M., Kern, C., Lehmann, T., Platt, U., Arellano, S., Hidalgo, S., 2010. Network for Observation of Volcanic and Atmospheric Change (NOVAC)—a global network for volcanic gas monitoring: network layout and instrument description. J. Geophys. Res. 115. https://doi.org/10.1029/2009JD011823.
Kern, C., Deutschmann, T., Vogel, L., Wöhrbach, M., Wagner, T., Platt, U., 2010. Radiative transfer corrections for accurate spectroscopic measurements of volcanic gas emissions. B Volc 72, 233–247. https://doi.org/10.1007/s00445-009-0313-7.
Kern, C., Deutschmann, T., Werner, C., Sutton, A.J., Elias, T., Kelly, P.J., 2012. Improving the accuracy of SO_2 column densities and emission rates obtained from upward-looking UV-spectroscopic measurements of volcanic plumes by taking realistic radiative transfer into account. J. Geophys. Res. 117, D20302. https://doi.org/10.1029/2012JD017936.
Koschmieder, H., 1925. Theorie der horizontalen sichtweite II: kontrast und sichtweite. Beiträge Phys. Freien Atmos. 12, 171–181.
Kunrat, S., Kern, C., Alfianti, H., Lerner, A.H., 2022. Forecasting explosions at Sinabung Volcano, Indonesia, based on SO_2 emission rates. Front. Earth Sci. https://doi.org/10.3389/feart.2022.976928.
Mather, T.A., 2015. Volcanoes and the environment: lessons for understanding Earth's past and future from studies of present-day volcanic emissions. J. Volcanol. Geotherm. Res. 304, 160–179. https://doi.org/10.1016/j.jvolgeores.2015.08.016.
Matsushima, N., Shinohara, H., 2006. Visible and invisible volcanic plumes. Geophys. Res. Lett. 33, L24309. https://doi.org/10.1029/2006GL026506.
McGonigle, A.J.S., Hilton, D.R., Fischer, T.P., Oppenheimer, C., 2005. Plume velocity determination for volcanic SO_2 flux measurements. Geophys. Res. Lett. 32. https://doi.org/10.1029/2005GL022470.
Millán, M.M., 1980. Remote sensing of air pollutants: a study of some atmospheric scattering effects. Atmos. Environ. 14 (11), 1241–1253. https://doi.org/10.1016/0004-6981(80)90226-7.
Mori, T., Mori, T., Kazahaya, K., Ohwada, M., Hirabayashi, J., Yoshikawa, S., 2006. Effect of UV scattering on SO_2 emission rate measurements. Geophys. Res. Lett. 33. https://doi.org/10.1029/2006GL026285.
Mulcahy, J.P., O'Dowd, C.D., Jennings, S.G., 2009. Aerosol optical depth in clean marine and continental Northeast Atlantic air. J. Geophys. Res. 114, D20204. https://doi.org/10.1029/2009JD011992.
Oppenheimer, C., Fischer, T., Scaillet, B., 2014. Volcanic degassing: Process and impact. In: Holland, H.D., Turekian, K.K. (Eds.), Treatise on Geochemistry, 2nd ed. Elsevier, pp. 111–179. https://doi.org/10.1016/B978-0-08-095975-7.00304-1.
Platt, U., Stutz, J., 2008. Differential Optical Absorption Spectroscopy: Principles and Applications. Springer, Berlin Heidelberg.
Trlica, A., Hutyra, L.R., Schaaf, C.L., Erb, A., Wang, J.A., 2017. Albedo land cover, and daytime surface temperature variation across an urbanized landscape. Earth's Future 5 (11). https://doi.org/10.1002/2017EF000569.
Wagner, T., Warnach, S., Beirle, S., Bobrowski, N., Jost, A., Puķīte, J., Theys, N., 2023. Investigation of three-dimensional radiative transfer effects for UV–Vis satellite and ground-based observations of volcanic plumes. Atmos. Meas. Tech. 16, 1609–1662. https://doi.org/10.5194/amt-16-1609-2023.
Williams-Jones, G., Stix, J., Hickson, C., 2008. The COSPEC cookbook: making SO_2 measurements at active volcanoes. IAVCEI Methods Volcanol. 1, 121–167. https://doi.org/10.13140/RG.2.2.13728.99845.